Hindawi
Journal of Sensors
Volume 2018, Article ID 7582605, 11 pages
https://doi.org/10.1155/2018/7582605

Research Article

Assessing the Difference in Measuring Bolt Stress: A Comparison of Two Optical Fiber Sensing Techniques

Jing Chai,[1,2] **Qi Liu**,[1] **Jinxuan Liu**,[1] **Guihua Zhang**,[1] **Dingding Zhang**,[1,2] **and Fengqi Qiu**[1]

[1]*School of Energy, Xi'an University of Science and Technology, Xi'an, Shaanxi 710054, China*
[2]*Key Laboratory of Western Mine Exploitation and Hazard Prevention, Ministry of Education, Xi'an, Shaanxi 710054, China*

Correspondence should be addressed to Jing Chai; chaij@xust.edu.cn and Qi Liu; lqxust@163.com

Received 28 February 2018; Revised 17 April 2018; Accepted 6 May 2018; Published 12 June 2018

Academic Editor: Romeo Bernini

Monitoring the load level of the rock bolts is of great importance for assessing risk. Based on the mechanical transmission mechanism of grouting bolts, the bolt pull-out test was carried out in lab. The performance of the bolt under pull-out loading was measured using the pulse-pre-pump Brillouin optical time domain analysis (PPP-BOTDA) and fiber Bragg grating (FBG) sensing technologies. The distribution characteristic of axial stress along the bolt was analysed in combination with the measurements obtained by the two sensing technologies. The relative standard deviation for repeatability errors in the determination and the setting time of resin grout was investigated. The results show that the distribution of axial stress is nonuniform along the anchorage section. The maximum value of axial stress on the bolt is closed to the pull-out side. The relative standard deviation for repeatability errors obtained by PPP-BOTDA is less than that obtained by FBG. The comparison of the measurements obtained by the two methods indicates that when the drawing force is greater than 20 kN and the axial stress is more than 10 kN, the two methods have better consistency. In the field application, it is necessary to estimate the deformation of matrix, leaving at least 500 minutes for resin bond to work.

1. Introduction

Rock bolts are part of the rock reinforcing system and are applied to reinforce the stability of rock strata and resist possible deformation [1]. A critical element of the supporting systems, rock bolts are widely utilized to stabilize and support engineering structures in some areas, such as underground mining, civil projects, and underground engineering [2, 3]. Accidents caused by the deformation of roadway surrounding rock and collapse of the roof in underground coal mining are common problems [4, 5]. The accidents often lead to workers getting injured or disabled, or in the worst scenario, casualties. At the same time, the effects to the mining company are detrimental—an extension of construction, operations being interrupted, and malfunctioning equipment [6].

The bolting system includes a borehole with a steel rebar element inserted into it. The borehole is enclosed in a capsule form with cement or resin grout and connected to the excavation surface by utilizing a nut and face plate assembly. Rock bolts are monitored to make sure they are functioning properly. In the field, rock bolts usually experience tensile and shear loading. When the reinforced rock mass deforms, a load transfer mechanism takes place between the bolt and the rock surface and transfers the applied tensile and shear load into the surrounding mass. Rock bolts may fail either at the grout–rock interface, in the grout medium, or at the bolt–grout interface. The identification of the shear stress distribution of the bonding interface is of great importance for understanding the load transfer mechanism and the optimal design of the rock bolts. Smart sensing technology is required to determine a fully grouted rock bolt with load distribution of high variance and complexity.

Different approaches are developed to ensure the rock bolt's integrity. The conventional method to evaluate rock bolt is electrical-resistance strain gauges, which is an effective indicator for a relatively shorter period of load measurement [7]. However, there are some shortcomings of traditional electric sensors in complex environmental applications, especially the presence of water around the rock. The advantages related to optical fiber sensors are not limited to being

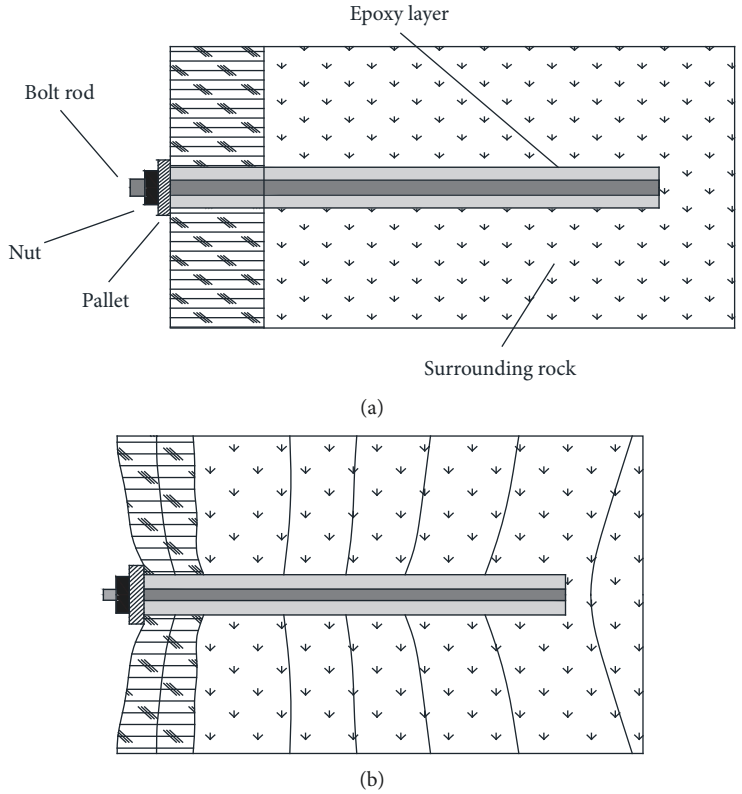

Figure 1: (a) Initial state of the bolt and (b) interaction of bolt with its surrounding rock mass.

Table 1: Mechanical parameters of bolt, resin, and concrete.

Properties	Density (kg/m^3)	Bulk modulus (GPa)	Shear modulus (GPa)	Cohesion (MPa)	Internal friction angle (°)	Tensile strength (MPa)
Bolt	7900	157	75	—	—	—
Resin	2000	5.2	2.8	8.5	31	5.3
Concrete	3200	3.9	2.5	3.7	26	2.2

immune to electromagnetic interference, reduced volume, and mass. The optical fiber sensors can also be multiplexed, meaning that more than one sensor can be integrated along a single optical fiber one can monitor. And optical fiber sensors can be used to measure temperature, humidity, and other physical quantities [8, 9].

Nellen et al. [10] embedded FBG sensors in the GFRP rock bolts in order to conduct pultrusion. The tensile evaluations showed that the embedded FBG sensors were capable of withstanding a high strain of 1.5%. FBG sensors are also applied to monitor the axial stress of rock bolts throughout the process of constructing underground tunnels by utilizing pilot models and investigating the load transfer principle of the ground anchor and tensile force distribution along the tendon [11, 12]. Iten and Puzrin [13] utilized the Brillouin optical time domain analysis (BOTDA) optical fiber-distributed sensing tactic for measuring the stress distribution along ground anchors. Moffat et al. [14] attempted to verify the BOTDA tactic through monitoring rock bolt loading conditions. Liu et al. [15] applied the dynamic distributed measurement capability of the PPP-BOTDA to monitor the structural damage under in-service operations. The BOTDA and fiber Bragg grating (FBG) sensing technology have been used to measure the stress distribution along the bolt [16]. However, in practical applications, the applicable measurement range and repeatability of the two methods need to be further studied.

In this study, the test apparatus for interfacial mechanics was developed to study the distribution characteristic of axial stress of the bolt. BOTDA sensors and FBG sensors were assessed during the bolt pull-out experiment. The repeatability errors of the two optical fiber sensing technologies were analysed, and the measurements at the same position were compared to determine the applicability of the two methods in monitoring the stress distribution of the bolt.

2. Principle

Based on the BOTDA sensing technology, PPP-BOTDA further improves the accuracy of Brillouin frequency

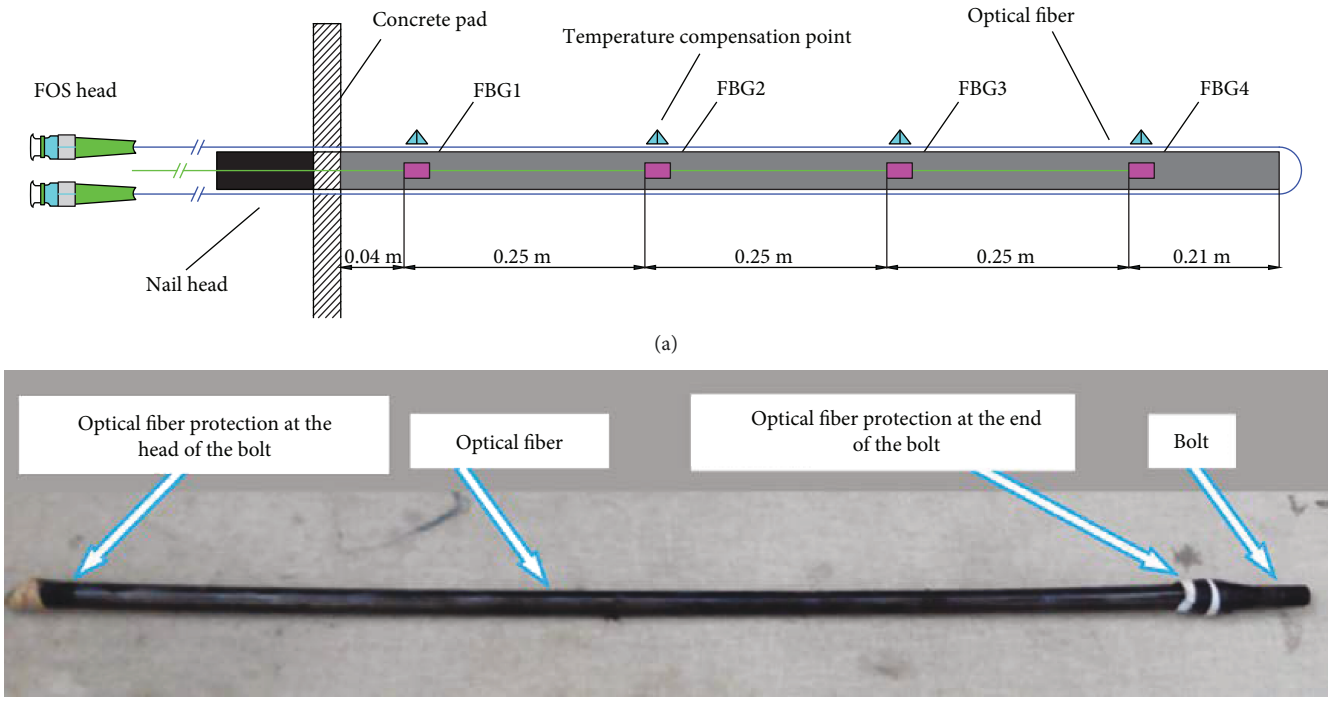

Figure 2: (a) Diagram of the sensors installation along the bolt and (b) photo of the installation of the sensors in the bolt.

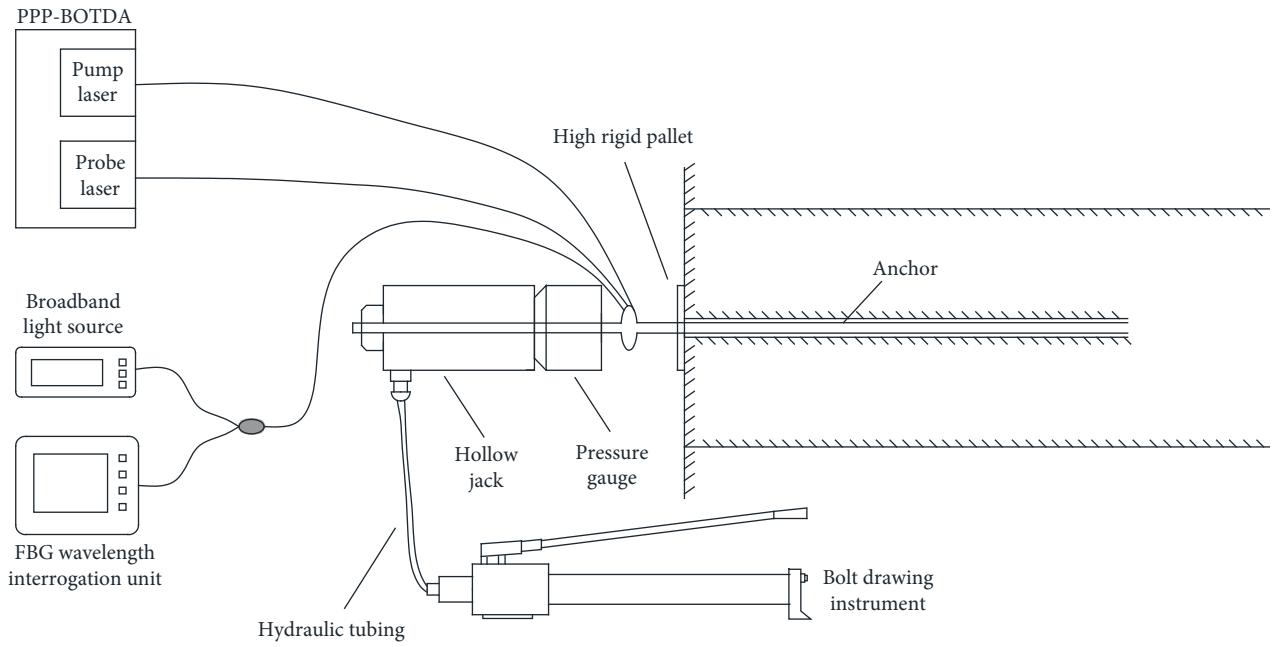

Figure 3: Schematic diagram of pull-out test setup.

identification that generates a broad bandwidth pulse before a narrow bandwidth one arrives. The PPP-BOTDA works on the principle of the stimulated Brillouin scattering effect, which is that a light photon interacts with an acoustic wave in an optical fiber. A pumping pulse light and a continuous wave probe light is injected into opposite ends of the optical fiber, respectively, in order to ensure that it spreads in the opposite direction. These two lights interact nonlinearly and excite an acoustic wave, which then couples the two optical waves to one another. The intensity of the Brillouin scattering signal is increased as the frequency difference between the pump and probe waves gets infinitely close to the Brillouin frequency of the optical fiber.

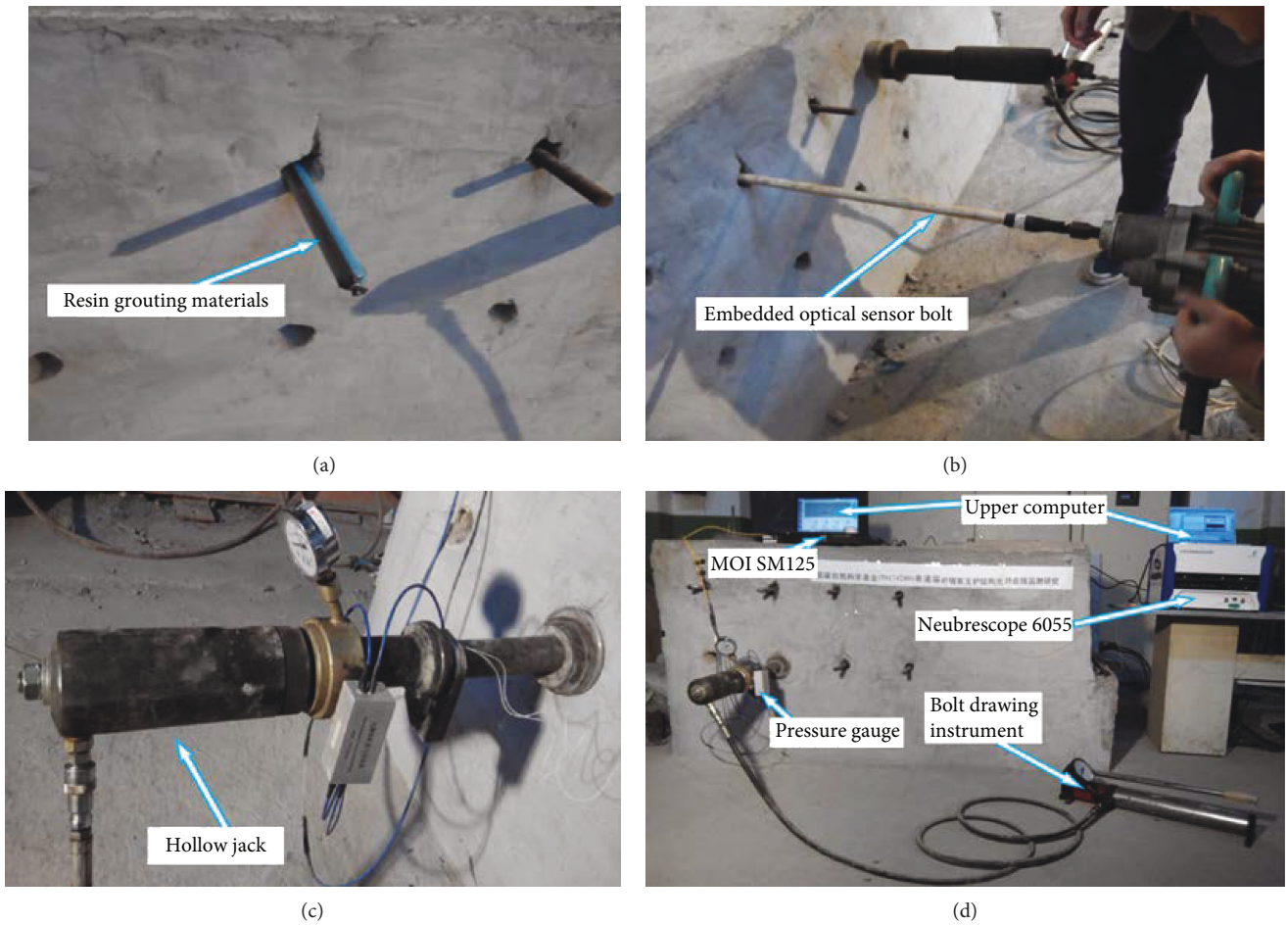

Figure 4: Photographs of the installation of a bolt pull-out test system. Installation of (a) resin grouting materials, (b) bolt encapsulated optical fiber sensors, and (c) hollow jack together with a pressure gauge. (d) A bolt pull-out test system after installation.

A Brillouin optical analysis system is utilized for stimulating and obtaining frequency data from Brillouin backscattered light, a product of the power light pulse that spreads along the fiber. At room temperature, the change of Brillouin frequency, $\Delta\nu_B$, reveals a linear dependence on the strain and temperature change. The frequency of the Brillouin scattering, strains, and temperature at different positions along a fiber are shown in the equation below.

$$\Delta\nu_B = C_\varepsilon \Delta\varepsilon + C_T \Delta T, \tag{1}$$

where $\Delta\varepsilon$ and ΔT are the strain and temperature changes in reference to their initial conditions, respectively. C_ε and C_T are strain- and temperature-sensitive coefficients, respectively.

The strain distribution $\varepsilon(x,t)$, changed with time at different positions along an optical fiber, can be written by

$$\varepsilon(x,t) = \varepsilon_i(x,t_i) + \frac{1}{C_\varepsilon}\nu_B(x,\varepsilon,t) - \frac{1}{C_\varepsilon}\nu_B(x,\varepsilon_i,t_i), \tag{2}$$

where x, t_i, and ε_i represent the position along an optical fiber, the time at the beginning of the test, and the initial strain, respectively. When there is any strain change on the optical fiber, the PPP-BOTDA spectrum can show the position of changes according to the above principle. The temperature- and strain-sensitive coefficients were measured and obtained 1.2 MHz/°C and 0.05 MHz/$\mu\varepsilon$, respectively.

Bragg grating can be inscribed into an optical fiber by multiple methods. The form of a series of grating planes along the fiber axis can be carried out by a refractive index modulation within an optical fiber core. When a broad band pulse is propagated down the fiber, a narrow-band pulse is reflected while the rest is transmitted. This narrow-band pulse is called the Bragg reflection with a centre wavelength λ_B.

$$\lambda_B = 2n_{eff}\Lambda_B, \tag{3}$$

where n_{eff}represents the effective refractive index and λ_B is the spatial period of the FBG.

The relative strength of the two changes differs according to which subjected perturbation the grating has, respectively. In the majority of the cases, the effect due to changes in the effective refractive index plays a dominant role. An axial strain in the grating alters not only the grating spatial period but also the effective refractive index and changes the Bragg wavelength as a result of the elastic behavior and the elastooptical effect. What is more, changing the

ambient temperature also leads to this due to the thermal expansion and the thermooptic effect. The equation displaying the extent to which the Bragg wavelength has shifted is as follows.

$$\frac{\Delta\lambda_B}{\lambda_B} = (1 - P_e)\varepsilon + [(1 - P_e)\alpha + \zeta]\Delta T, \quad (4)$$

where P_e represents the photoelastic constant of the fiber, ε is the axial strain, ζ is the thermooptic coefficient of the fiber, α is the fiber thermal-expansion coefficient, and ΔT is the change of temperature. $\Delta\lambda_B$ can be linear to the strain change with the temperature fixed, because the FBG sensor is only sensitive for strain and temperature. The thermal and strain coefficients are 10.3 pm/°C and 1.21 pm/$\mu\varepsilon$ for FBG sensors, respectively.

The response of tensile mechanics will be generated in the bolt pull-out test when the end of the bolt is exerted by an external force. The bolt body is pulled, which will produce shear mechanical effects between bolt and bonding materials. The corresponding points' axial stress can be calculated by the strain value of the bolt body,

$$N_i = \frac{1}{4}\pi D^2 E\varepsilon_i, \quad (5)$$

where N_i is the axial stress of the strain gauge of point i, D is the diameter of the bolt, E is the elastic modulus of the bolt, and ε_i is the strain value of point i.

To assess the repeatability of the two optical sensing methods in the bolt pull-out test, the relative standard deviation was used. The average of one sample in replicate tests can be given as

$$\bar{x} = \frac{1}{q}\sum_{j=1}^{q} x, \quad (6)$$

where x is the wavelength shift of the FBG sensor or Brillouin frequency shift of the PPP-BOTDA sensor, q is the number of tests, and $\bar{x}$ is the mean value of wavelength shift of the FBG sensor or Brillouin frequency shift of the PPP-BOTDA sensor.

The standard deviation of this sample can be expressed as follows,

$$S = \sqrt{\frac{\sum_{j=1}^{q}(x_j - \bar{x})^2}{q - 1}}, \quad (7)$$

where S is the standard deviation.

The relative standard deviation of this sample can be obtained as

$$\mathrm{RSD} = \frac{s}{\bar{x}}, \quad (8)$$

where RSD is the relative standard deviation.

3. Experimental Program

In this test, the fully resin-grouted bolts are used. The mechanism behind the fully resin-grouted bolts is that resin bonds

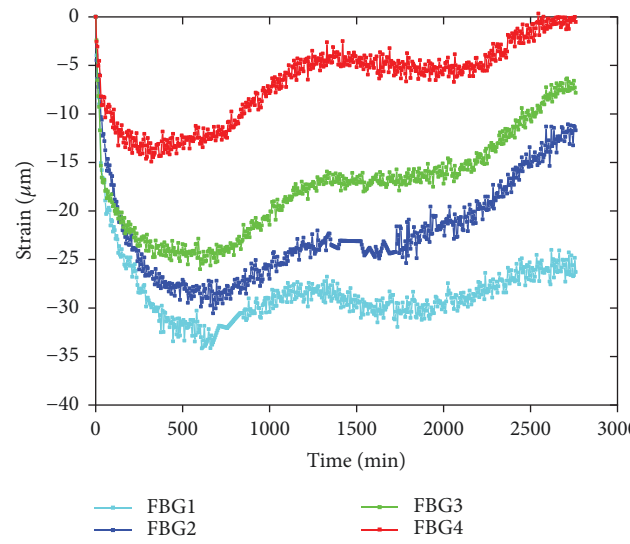

Figure 5: The strain monitoring results versus time during the solidification of resin.

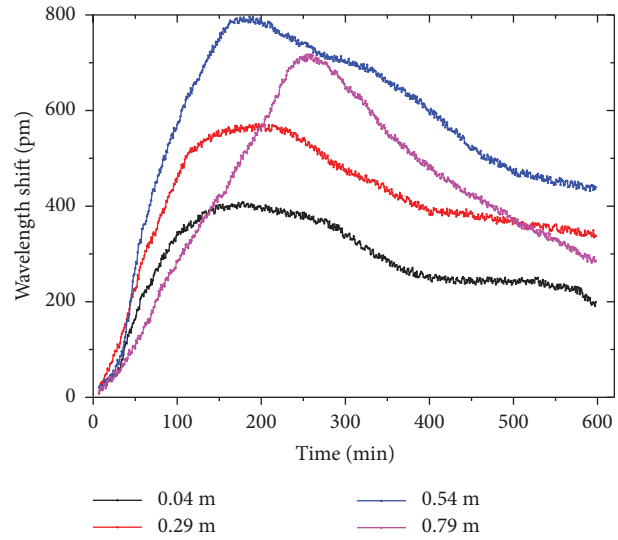

Figure 6: The wavelength shift of FBG temperature sensors versus time during the solidification of resin.

the entire bolt to the concrete or rock mass. Compared with other types of bolts, it is an advantage to use fully resin-grouted bolts in long-term or permanent projects because the bonding material between the bolt and the concrete protects the bolt from the moisture. The use of the resin bonding agent achieves the fast installation as compared to the other types of bonding bolts.

The anchorage body consists of three main components, two ancillary parts and two bonding interfaces. The three main components are including bolt, bonding materials, and concrete. The two ancillary parts are including nut and pallet. The two bonding interfaces are including the bolt-grout interface and the grout-concrete interface, as is shown in Figure 1(a). When the bolt is pulled, the axial loading's

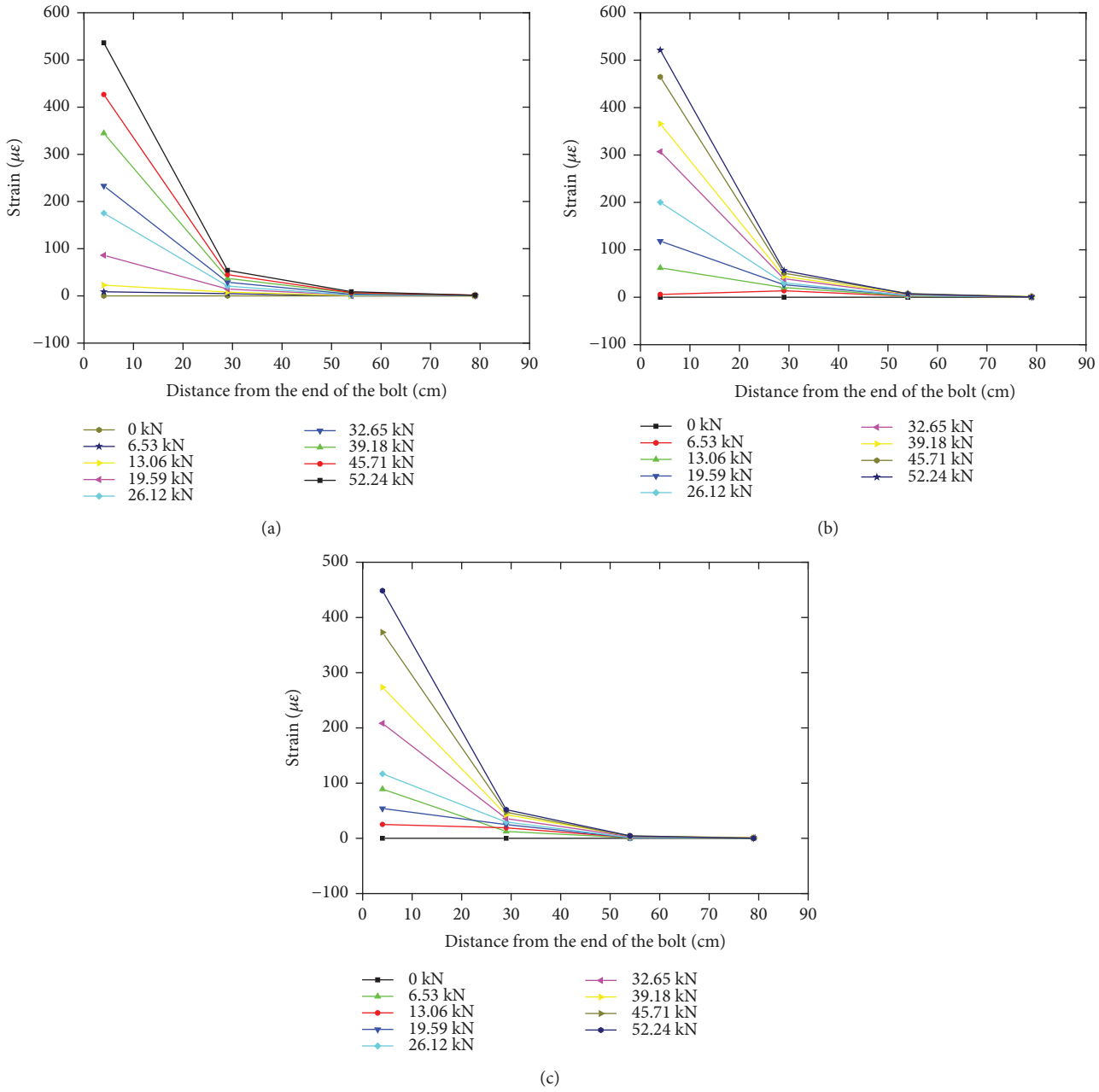

Figure 7: The strain monitoring results obtained by the FBG sensors on the bolt in three pull-out tests: (a) the first cycle, (b) the second cycle, and (c) the third cycle.

transmission is from the bolt body to grouting agent and then to concrete. More specifically, a bolt, installed in a deformable concrete, is exerted by an axial force; the bolt resists the movement of concrete through shear stresses generated axially in the interface between bolt and bonding materials, as is shown in Figure 1(b).

In this study, the distributed strain sensing optical fiber and the fiber Bragg grating sensor are used to measure stress changes on the bolt. The distributed strain sensing optical fiber is a single-mode fiber with a diameter of 0.9 mm, and its maximum bending radius ranges between 9 and 16 mm. The grating length of the FBG is 10 mm. The FBG sensors are connected together and share a transmission fiber. The bolt is made of cold drawn steel with a diameter of 18 mm, and its length is 1.1 m. Poisson's ratio of the bolt is 0.2. The basic parameters of these three components are listed in Table 1.

A *U*-shaped distribution of a strain sensing optical fiber is used to obtain detailed information on the stress of bolt in the experimental process. The layout of the monitoring system on the bolt is shown in Figure 2.

The optical fiber was pretensioned and adhered to the surface of the bolt by an approximately 2 mm layer of cyanoacrylate adhesives, which can serve as cover to protect the optical

fiber against accidental damage during the experiments. As the FBG sensor can be affected by the temperature, additional temperature sensors were used to be temperature-corrected.

The experimental device includes a Micron Optics SM125 interrogator, a PPP-BOTDA interrogator, a pressure gauge, and a bolt drawing instrument, as is shown in Figure 3. The strains on the bolt were measured by the distributed fiber optical sensor with the Neubrescope (Neubrex, model: NBX-6055) and by the FBG sensors with an optical spectrum interrogator (MOI, model: SM125). The measurement wavelength of the interrogator ranges from 1510 nm to 1590 nm. The measurement accuracy and repeatability are 1 pm and 0.5 pm, respectively. The fiber formed a loop with the Neubrescope for measurement, and its sampling interval and spatial resolution were set as 1 cm and 5 cm, respectively.

The concrete mixture block with dimensions of $2000 \times 1100 \times 800$ mm was built, which was made up of normal Portland cement, natural sand, and water with a ratio of 1 : 1 : 0.5. The minimum and maximum particle sizes of natural sand were 3 mm and 18 mm, respectively. After casting, the concrete mixture block was maintained for three months. The installation of resin grouting bolts includes the drilling of holes, resin implantation, and bolt installation. A resin cartridge includes resin and a catalyst in different sections. Figure 4 depicts how the cartridges are inserted into the borehole and how the bolt shaft is revolved into the cartridges. Spinning the bolt shaft breaks the plastic sheath of the cartridges, mixing the resin and catalyst. Two varying cartridges were utilized, with the fast-setting one further in the borehole and in front of the slow-setting one.

After installation, the tests were started 5 days later. The pull-out test procedure consisted of three loading/unloading cycles, and the drawing forces of 6.53, 13.06, 19.59, 26.12, 32.65, 39.18, 45.71, and 52.24 kN were applied to the bolt. During the test, one end of the bolt was pulled longitudinally by the bolt drawing instrument. In each step, the load was kept constant for 5 min to make sure that the readings from the optical fibers were stable. The readings from the distributed fiber optical sensor and the FBG sensors were recorded by the Neubrescope and the optical spectrum interrogator, respectively.

4. Results and Discussions

After the installation of the bolt, the resin bonding agent expanded due to chemical reaction, which interacted with the surrounding concrete and the bolt. The plot in Figure 5 presents the results on the variation of axial stress on the bolt, which shows the strain as a function of the time the bolt was installed in the borehole. In all the responses presented, a similar trend was observed where the strain on the bolt rapidly increased first and then gradually reduced. The time taken for the strain at 79 cm from the orifice to reach the maximum after the installation of the bolt is approximately 350 min. The time taken for the strain at 4, 29, and 54 cm from the orifice to reach the maximum after the installation of the bolt is approximately 500 min. At this time, the entire bolt is subjected to the maximum compressive stress because the interaction between the resin bonding agent and the surrounding matrix reaches the maximum. The wavelength shift of the FBG temperature sensors at different positions along the bolt is shown in Figure 6.

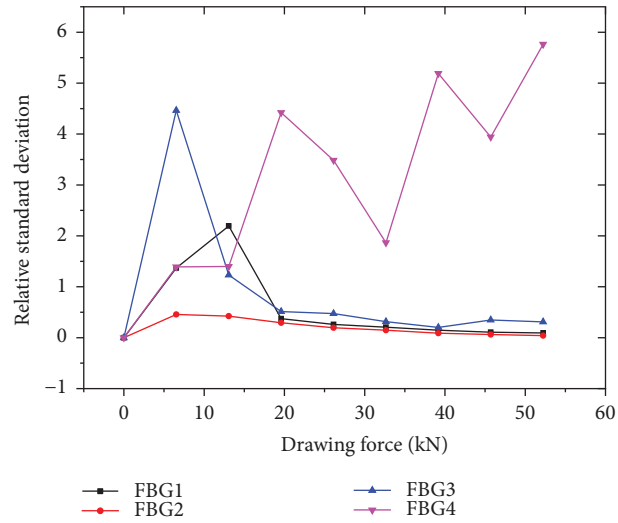

Figure 8: Relative standard deviation (RSD) of the FBG sensors for three repeated tests.

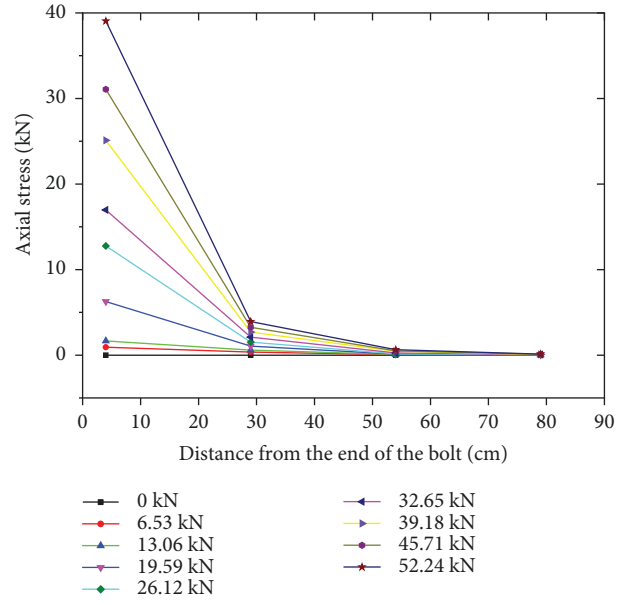

Figure 9: Average axial stress of three repeated tests measured by FBG sensors.

The maximum strain at different locations on the bolt is different, which means that the volume expansion of the resin bonding agent results in different compressive stresses at different locations on the bolt. Then, the strain gradually decreases, which means the interaction between the resin bonding agent and the surrounding matrix is complete. The strain at 79 cm from the orifice first restores to the initial value. Before the strain reaches the maximum, the interaction between the bonding agent and the surrounding matrix is not

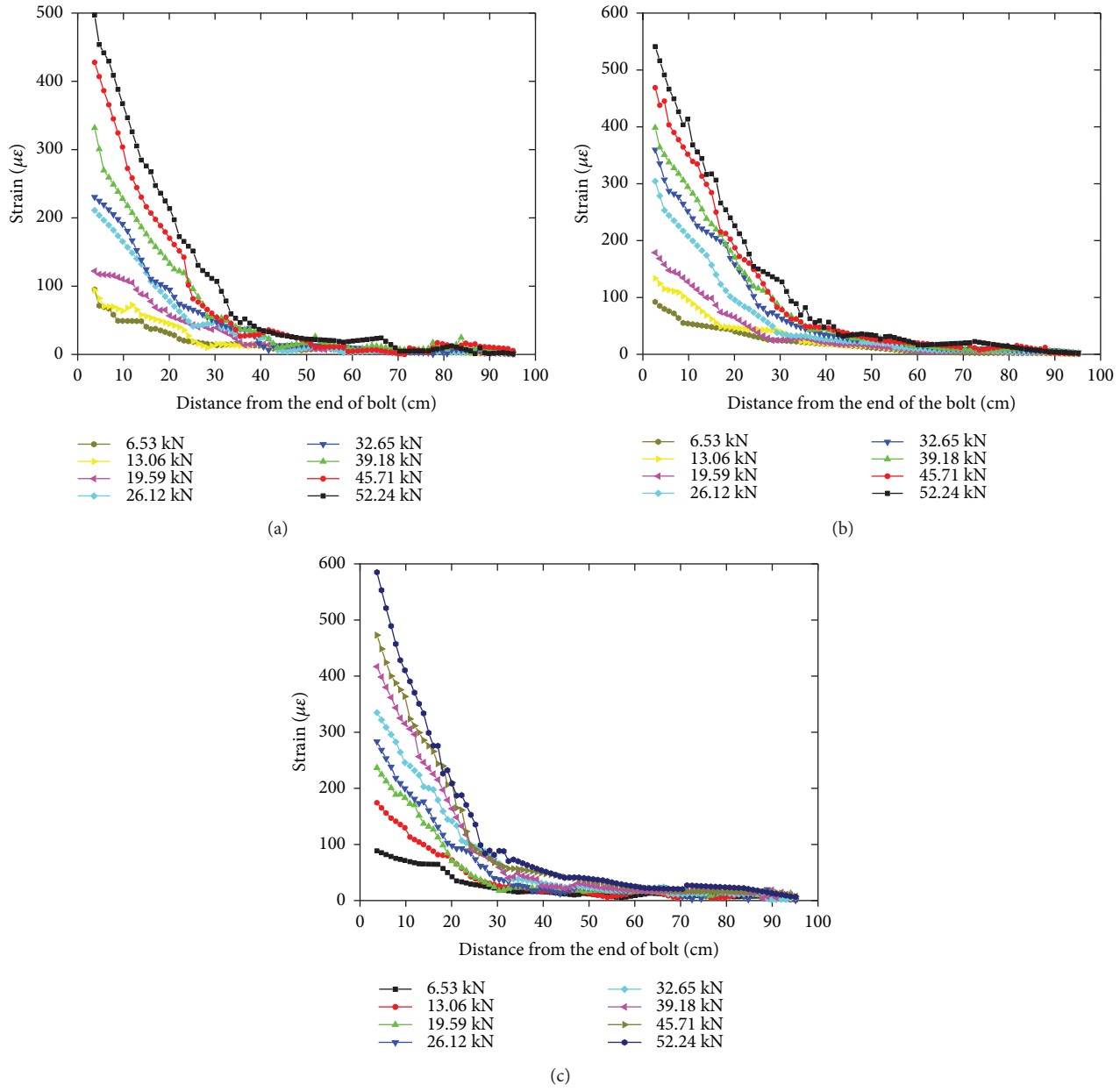

Figure 10: The strain monitoring results obtained by the PPP-BOTDA sensors on the bolt in three pull-out tests: (a) the first cycle, (b) the second cycle, and (c) the third cycle.

complete, and the anchoring effect is relatively weak. Some studies [1] show that it takes a resin bond only tens of minutes to set the bolt in place without considering the more interaction time between the resin bond and the surrounding matrix. However, this study shows that the resin bond does not interact completely with the surrounding matrix in tens of minutes, and it is necessary to predict the deformation of the matrix, leaving at least 500 minutes for the resin bond to work.

The distribution and transfer characteristics of the strain obtained by the FBG sensors along the bolt under different drawing forces are presented in Figure 7.

With the increase of the drawing force, the strain obtained by the FBG sensors along the bolt increases gradually, and the maximum strain obtained by the FBG sensors is on the pull-out side, while the amplitude of the strain decreases along the bolt toward the inside. As is shown in Figure 8, when the drawing force is greater than 20 kN, the relative standard deviation of the repeatability of the FBG sensors placed at 4, 29, and 54 cm from the orifice is less than 0.5, and the repeatability of the FBG sensors placed at these locations is better than that of the FBG sensor placed at 79 cm from the orifice, which can be calculated by (6), (7), and (8). With the drawing force increasing, a trend can be observed where the relative standard deviation of the repeatability of the FBG sensor, placed at 79 cm, has a further increase. When the drawing force is less than 20 kN, in addition to the sensor placed at 29 cm, the relative standard

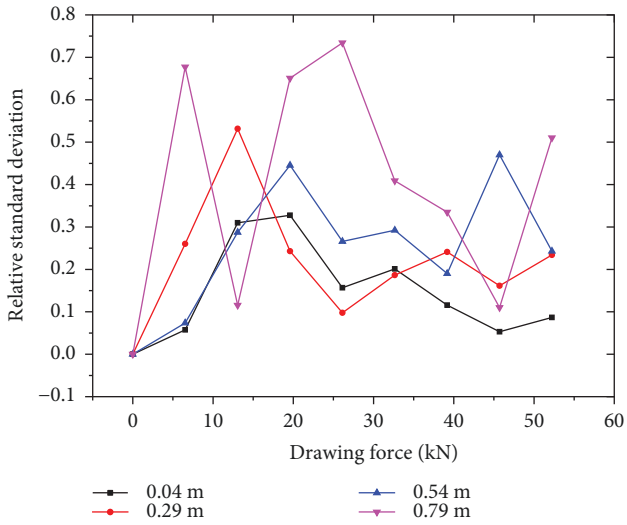

Figure 11: Relative standard deviation (RSD) of the PPP-BOTDA sensors for three repeated tests.

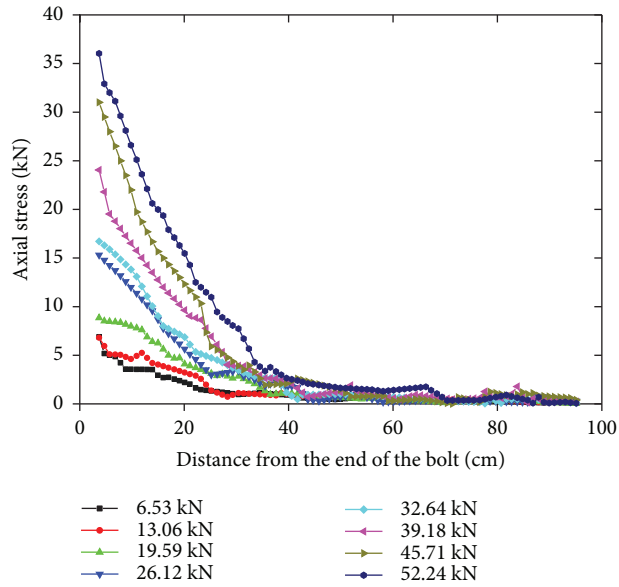

Figure 12: Average axial stress of three repeated tests measured by PPP-BOTDA sensors.

deviation of the repeatability of the other sensors is greater than 1. This indicates that the repeatability of the FBG sensor is poor at lower drawing forces. Using the average of the three measurements obtained by FBG sensors, the axial stress distribution along the bolt can be calculated by (3), (4), and (5), as shown in Figure 9.

The distribution and transfer characteristics of the strain obtained by the PPP-BOTDA along the bolt under different drawing forces are presented in Figure 10.

With the increase of the drawing force, the strain obtained by the PPP-BOTDA sensors along the bolt increases gradually, and the maximum strain obtained by the PPP-BOTDA sensors is on the pull-out side, while the amplitude of the strain decreases along the bolt toward the inside. The strain located at 75 cm from the orifice along the bolt begins to drop to near 0, which is also close to 0 from here to the end of the bolt. With the increase of the drawing force, this position does not change.

As is shown in Figure 11, the relative standard deviation of the repeatability of the PPP-BOTDA sensors along the bolt is less than 0.8. The repeatability of the PPP-BOTDA sensors is better than that of the FBG sensors. Using the average of the three measurements obtained by PPP-BOTDA sensors, the axial stress distribution along the bolt can be calculated by (1), (2) and (5), as shown in Figure 12. The axial stress of the bolt measured by the FBG and PPP-BOTDA sensors are different. When the drawing force is less than 32.64 kN, the axial stress obtained by the PPP-BOTDA sensors at the orifice is closer to the pull force. When the drawing force is 32.64 kN, the axial stress obtained by the PPP-BOTDA sensors at the orifice is equal to that of PPP-BOTDA. When the drawing force is greater than 32.64 kN, the axial stress obtained by the FBG sensors at the orifice is closer to the pull force.

The ratio between the axial stress measured by the FBG sensor and the PPP-BOTDA sensor indicates the degree of deviation on the measured values obtained by the two optical sensing methods at the same position on the bolt. With the drawing force increasing, a trend can be observed where the ratio of axial stress obtained by the PPP-BOTDA and FBG sensors has a further decrease at the same position of the bolt, as is shown in Figure 13.

When the axial stress on the bolt at 4 cm from the orifice ranges from 0 to 10 kN, the ratio is 1.5–7.5. When the axial stress ranges from 10 to 40 kN, the ratio is 1.0–1.5. With the drawing force increasing, the measurements obtained by the PPP-BOTDA and FBG sensors monotonously increase and get closer. When the axial stress on the bolt at 29 cm from the orifice ranges from 0 to 9 kN, the ratio is 1.3–2.8. When the axial stress on the bolt at 54 cm from the orifice ranges from 0 to 1.6 kN, the ratio is 1.5–13. When the axial stress on the bolt at 79 cm from the orifice ranges from 0 to 1.4 kN, the ratio is 4–14.5.

As the drawing force increases, the change in the measurements obtained by the FBG sensor and the PPP-BOTDA sensor is different; one is monotonically increasing and the other is fluctuating on the bolt at 29/54/79 cm. The smaller the axial stress, the greater the deviation of the measurements obtained by the two optical sensing methods. When the axial stress is less than 10 kN, the measured value of the PPP-BOTDA sensors is greater than that of the FBG sensors. The comparison of the measurements obtained by the two methods indicates that when the drawing force is greater than 20 kN and the axial stress is more than 10 kN, the two methods have better applicability. The repeatability error of the measurement is small, and the measurement values of the two measurement methods are almost the same.

5. Conclusion

In this paper, the performance of the bolt under pull-out loading was studied using the PPP-BOTDA and FBG sensing technologies. The distribution characteristic of axial stress along the bolt was analysed in combination with the

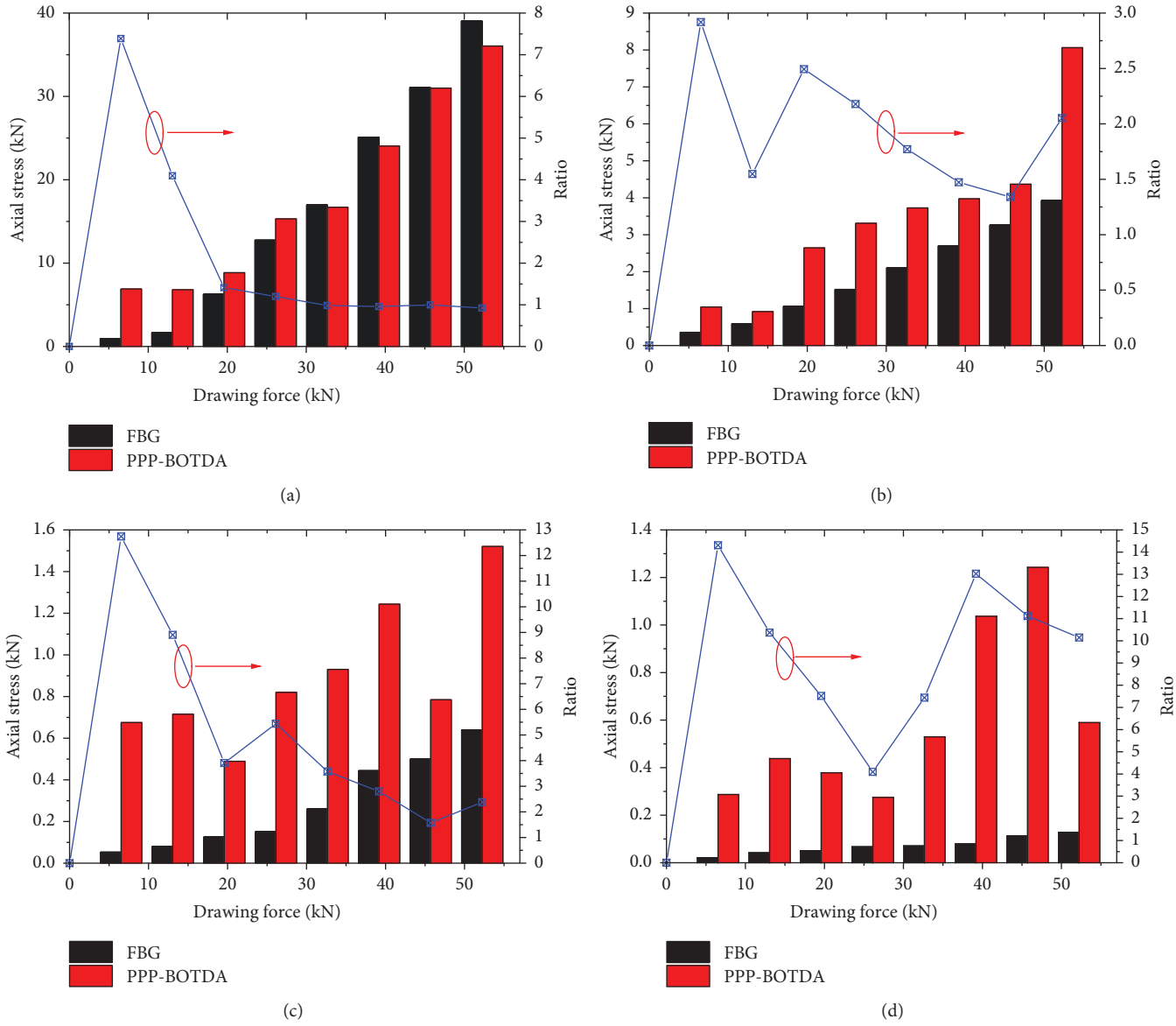

Figure 13: Axial stress obtained by the FBG and PPP-BOTDA sensors and its ratio, located at (a) 4 cm, (b) 29 cm, (c) 54 cm, and (d) 79 cm from the orifice on the bolt.

measurements obtained by the two optical sensing technologies. The relative standard deviation for repeatability errors in the determination and the setting time of the resin-grout was investigated. After the installation of the bolt, the resin bonding agent expands due to chemical reaction, which interacts with the surrounding concrete and the bolt. The Bragg wavelength of FBG sensors installed on the bolt changes as a function of time. Before the wavelength shift of the FBG reaches the maximum, the interaction between the bonding agent and the surrounding matrix is not complete, and the anchoring effect is relatively weak. In the field application, it is necessary to estimate the deformation of the matrix, leaving at least 500 minutes for the resin bond to work. When the drawing force is greater than 20 kN, the relative standard deviation of the repeatability of the sensor placed at 4, 29, and 54 cm from the orifice is less than 0.5, and the repeatability of measurement at these locations is better than that of the sensor placed at 79 cm from the orifice.

Through the three bolt pull-out tests, the relative standard deviation of the repeatability of the measurements obtained by PPP-BOTDA is less than 0.8. Compared with the measurements of the FBG sensor, the repeatability of the measurements by PPP-BOTDA is better. The smaller the axial stress, the greater the deviation of the measurements obtained by the two methods. When the axial stress is less than 10 kN, the measured value of PPP-BOTDA is greater than that of the FBG sensor. The comparison of the measurements obtained by the two methods indicates that when the drawing force is greater than 20 kN and the axial stress is more than 10 kN, the two methods have better applicability. The repeatability error of the measurement is small, and the measurement values of the two

measurement methods are almost the same. When the drawing force is less than 20 kN and the axial stress is less than 10 kN, the applicability of these two measurement methods remains to be further studied.

Conflicts of Interest

The authors declare that they have no conflicts of interest.

Acknowledgments

This work was supported by the Natural Science Foundation of China (NSFC, no. 41027002) and the Doctoral Scientific Fund Project of the Chinese Ministry of Education (no. 20126121110003). The authors sincerely appreciate the financial supports of NSFC and the Chinese Ministry of Education. Thanks are also due to the graduated students of Xi'an University of Science and Technology; this study would not to be so smoothly implemented without them.

References

[1] G. Song, W. Li, B. Wang, and S. Ho, "A review of rock bolt monitoring using smart sensors," *Sensors*, vol. 17, no. 4, p. 776, 2017.

[2] M. Ghadimi, K. Shahriar, and H. Jalalifar, "A new analytical solution for the displacement of fully grouted rock bolt in rock joints and experimental and numerical verifications," *Tunnelling and Underground Space Technology*, vol. 50, pp. 143–151, 2015.

[3] G. Wang, X. Wu, Y. Jiang, N. Huang, and S. Wang, "Quasi-static laboratory testing of a new rock bolt for energy-absorbing applications," *Tunnelling and Underground Space Technology*, vol. 38, pp. 122–128, 2013.

[4] D.-s. Xu and J.-h. Yin, "Analysis of excavation induced stress distributions of GFRP anchors in a soil slope using distributed fiber optic sensors," *Engineering Geology*, vol. 213, pp. 55–63, 2016.

[5] S. C. M. Ho, W. Li, B. Wang, and G. Song, "A load measuring anchor plate for rock bolt using fiber optic sensor," *Smart Materials and Structures*, vol. 26, no. 5, article 057003, 2017.

[6] H. S. B. Duzgun and H. H. Einstein, "Assessment and management of roof fall risks in underground coal mines," *Safety Science*, vol. 42, no. 1, pp. 23–41, 2004.

[7] T.-b. Zhao, W. Y. Guo, Y. C. Yin, and Y. L. Tan, "Bolt pull-out tests of anchorage body under different loading rates," *Shock and Vibration*, vol. 2015, Article ID 121673, 8 pages, 2015.

[8] J. Chai, Q. Liu, J. Liu, and D. Zhang, "Optical fiber sensors based on novel polyimide for humidity monitoring of building materials," *Optical Fiber Technology*, vol. 41, pp. 40–47, 2018.

[9] F. Li, Y. du, W. Zhang, and F. Li, "Fiber Bragg grating soil-pressure sensor based on dual L-shaped levers," *Optical Engineering*, vol. 52, no. 1, article 014403, 2013.

[10] A. Frank, P. M. Nellen, R. Broennimann, and U. J. Sennhauser, "Fiber optic Bragg grating sensors embedded in GFRP rock-bolts," *Smart Structures and Materials 1999: Sensory Phenomena and Measurement Instrumentation for Smart Structures and Materials*, vol. 3670, pp. 497–505, 1999.

[11] X. Weng, H. Ma, and J. Wang, "Stress monitoring for anchor rods system in subway tunnel using FBG technology," *Advances in Materials Science and Engineering*, vol. 2015, Article ID 480184, 7 pages, 2015.

[12] T. M. Do and Y.-S. Kim, "Prediction of load transfer depth for cost-effective design of ground anchors using FBG sensors embedded tendon and numerical analysis," *Geomechanics and Engineering*, vol. 10, no. 6, pp. 737–755, 2016.

[13] M. Iten and A. M. Puzrin, "BOTDA road-embedded strain sensing system for landslide boundary localization," in *Smart Sensor Phenomena, Technology, Networks, and Systems 2009*, vol. 7293, p. 729316-729316, 2009.

[14] R. A. Moffat, J. F. Beltran, and R. Herrera, "Applications of BOTDR fiber optics to the monitoring of underground structures," *Geomechanics and Engineering*, vol. 9, no. 3, pp. 397–414, 2015.

[15] R. M. Liu, S. K. Babanajad, T. Taylor, and F. Ansari, "Experimental study on structural defect detection by monitoring distributed dynamic strain," *Smart Materials and Structures*, vol. 24, no. 11, article 115038, 2015.

[16] B. Forbes, N. Vlachopoulos, A. J. Hyett, and M. S. Diederichs, "A new optical sensing technique for monitoring shear of rock bolts," *Tunnelling and Underground Space Technology*, vol. 66, pp. 34–46, 2017.